Journal of Blood and Biotherapy

ISSN: 3135-0496 (Print) | 3135-050X (Online)

Hematology • Transfusion Medicine • Blood • Biotherapy

About the Journal

Hosted by the International Association of Asia-Pacific Blood Types and Genomics (IAABG), Journal of Blood and Biotherapy (JOFBBT) publishes high-quality research to advance science and innovation in hematology, transfusion medicine, and biotherapeutics. With a core commitment to fostering interdisciplinary collaboration, it brings together researchers, clinicians, and industry partners to solve key problems in blood disorders, cellular therapies, and biological treatments. A key focus is on translational research, ensuring that scientific discoveries are effectively translated into clinical applications that improve patient care globally.

◎ Register as Reader, Author or Reviewer

Create your account on our website to stay updated, submit your next manuscript, or contribute your expertise as a reviewer. All roles are welcomed and valued.

Contact & Connect

Email: office@jofbbt.com

Website: https://www.jofbbt.com

IAABG

Accepted: 29 April 2026

DOI: 10.46701/jbbt260502

Journal of Blood and Biotherapy

IAABG

ARTICLE

Integrative transcriptomic and clinical cohort analysis identifies immunometabolic prognostic signatures in multiple myeloma

Song Jin[1,†] | Lijun Song[2,†] | Qian Xu[3,4] | Tiantian Zhang[5] | Li Wang[5] | Yuping Wei[2] | Haitao Wang[5] | Chao Ma[5] | Hongqi Yang[3,4]

[1]Translational Medicine Research Center, Medical Innovation Research Division of The Fourth Medical Center of Chinese PLA General Hospital, Beijing 100048, China

[2]Department of Hematology, People's Hospital of Ningxia Hui Autonomous Region, Yinchuan, Ningxia 750002, China

[3]Medical School of Chinese PLA, Beijing 100853, China

[4]Department of Health Economics, The Second Medical Center of Chinese PLA General Hospital, Beijing 100853, China

[5]Senior Department of Hematology, The Fifth Medical Center of Chinese PLA General Hospital, Beijing 100039, China

† These authors contributed equally to this work.

Correspondence

Chao Ma, Senior Department of Hematology, The Fifth Medical Center of Chinese PLA General Hospital, No. 28 Fuxing Road, Haidian District, Beijing 100039, China.
Email: ma000chao@126.com.

Hongqi Yang, Medical School of Chinese PLA; Department of Health Economics, The Second Medical Center of Chinese PLA General Hospital, No. 28 Fuxing Road, Haidian District, Beijing 100853, China.
Email: dylan301@126.com

Abstract

Background: Multiple myeloma (MM) exhibits considerable clinical heterogeneity; however, current prognostic models inadequately capture the immunometabolic dysregulation central to its pathogenesis. This study aims to characterize the immunometabolic landscape of MM through integrative transcriptomic and clinical cohort analysis and to identify robust prognostic signatures.

Methods: Transcriptomic data from the GSE24080 dataset (325 MM patients, 234 healthy controls) were analyzed to identify differentially expressed genes (DEGs), perform Kyoto Encyclopedia of Genes and Genomes (KEGG) pathway enrichment analysis, estimate immune cell infiltration using Cell-type Identification By Estimating Relative Subsets Of RNA Transcripts (CIBERSORT), and develop a molecular classifier *via* least absolute shrinkage and selection operator (LASSO) regression. A clinical cohort of 101 newly diagnosed MM patients was retrospectively enrolled to validate the clinical relevance of immunometabolic biomarkers. Baseline characteristics were compared across International Staging System (ISS) stages, Spearman correlation analysis was performed to explore inter-relationships among biomarkers, and Cox regression models were constructed to identify independent prognostic factors. Kaplan-Meier survival curves were generated for ISS stages and β_2-microglobulin (β_2-MG) risk categories.

Results: Transcriptomic analysis identified 342 upregulated and 112 downregulated DEGs in MM, with significant enrichment in the p53 and FOXO signaling pathways. Immune deconvolution revealed decreased naive B cells,

Funding information
This study was supported by the grants from the Program for Appropriate Technology Promotion of Ningxia Hui Autonomous Region Health Commission (Grant No. 2025-NWSY-A005), the Postdoctoral Fellowship Program of CPSF (Grant No. GZC20242288), and the People's Benefit Project of the Department of Science and Technology of Ningxia Hui Autonomous Region (Grant No. 2026CMG03010).

memory B cells, and $CD8^+$ T cells, alongside increased plasma cells, regulatory T cells (Tregs), monocytes, and macrophages in MM samples. Consensus clustering defined three distinct immunometabolic subtypes, and a 12-gene LASSO classifier demonstrated excellent diagnostic performance (area under the curve [AUC] = 0.979). In the clinical cohort (median age 63.2 years; 60% male), advanced ISS stage was associated with elevated β_2-MG levels ($p < 0.001$), reduced hemoglobin (HGB) concentration ($p < 0.001$), and an increased bone marrow plasma cell percentage (BMPC) ($p = 0.006$). Spearman analysis revealed strong negative correlations between β_2-MG and HGB ($\rho = -0.70$, $p < 0.001$) as well as between BMPC and HGB ($\rho = -0.48$, $p < 0.001$). Multivariate Cox regression identified age (hazard ratio [HR] = 1.041, 95% confidence interval [CI]: 1.004–1.079, $p = 0.029$), β_2-MG (HR = 1.065, 95% CI: 1.022–1.110, $p = 0.0027$), and HGB (HR = 0.978, 95% CI: 0.962–0.994, $p = 0.0089$) as independent prognostic factors. Kaplan-Meier analysis demonstrated significant survival stratification by both ISS stages and β_2-MG risk categories (log-rank $p < 0.001$ for both).

Conclusions: These findings suggest that β_2-MG and HGB, as surrogates of immunometabolic disturbance-driven tumor burden and hematopoietic suppression, offer potential avenues for improved risk stratification and the development of personalized therapeutic strategies in MM.

Keywords
multiple myeloma; immunometabolism; prognostic biomarkers; transcriptomics; β_2-microglobulin; LASSO regression

Highlights
- This study characterizes the immunometabolic landscape of multiple myeloma (MM), revealing p53/FOXO pathway enrichment, decreased naive B cells, and increased regulatory T cells (Tregs).
- A 12-gene LASSO classifier (area under the curve [AUC] = 0.979) defines three distinct immunometabolic subtypes in MM.
- β_2-microglobulin (β_2-MG) and hemoglobin (HGB) are independent prognostic factors for MM risk stratification.

1. INTRODUCTION

Multiple myeloma (MM) is the second most prevalent hematologic malignancy worldwide, accounting for approximately 10% of all hematologic cancers and characterized by the clonal proliferation of malignant plasma cells in the bone marrow [1–3]. The disease typically presents with a constellation of clinical manifestations collectively known as CRAB features: hypercalcemia, renal insufficiency, anemia, and osteolytic bone lesions [4, 5]. Over the past two decades, the therapeutic landscape for MM has been revolutionized by the introduction of novel agents, including proteasome inhibitors (PIs), immunomodulatory drugs (IMiDs), and monoclonal antibodies, which have substantially improved response rates and prolonged patient survival [6]. Despite these advancements, MM remains an incurable disease, with patient outcomes exhibiting remarkable heterogeneity—overall survival (OS) can range from several months to more than 20 years [7]. This clinical diversity underscores the critical need for accurate prognostic stratification to guide treatment decisions and to identify high-risk patients who may benefit from more intensive or alternative therapeutic approaches [8, 9].

The International Staging System (ISS), introduced in 2005, represents a significant advancement in MM prognostication by stratifying patients based on two readily available serum biomarkers: albumin and β_2-microglobulin (β_2-MG) [10]. Subsequently, the Revised International Staging System (R-ISS) incorporated high-risk cytogenetic abnormalities [del(17p), t(4;14), t(14;16)] and elevated lactate dehydrogenase levels to enhance prognostic accuracy [11]. While these staging systems have become the standard tools for risk stratification in clinical practice, they possess inherent limitations. The ISS fails to account for cytogenetic heterogeneity, and its prognostic performance has

diminished in the era of novel agents [12–14]. The R-ISS, although more comprehensive, assigns approximately 60% of patients to an intermediate-risk group (stage II) that exhibits substantial heterogeneity in clinical outcomes [15, 16]. More comprehensive systems, such as the Mayo mSMART 3.0, incorporate a broader spectrum of chromosomal abnormalities; however, their clinical adoption is limited by logistical constraints including high costs, restricted availability, and lack of standardization across centers [17]. Therefore, there remains an urgent need for more precise, accessible, and clinically applicable prognostic tools for MM.

Emerging evidence has highlighted the pivotal role of immune dysregulation and metabolic alterations in MM pathogenesis and progression [18]. The bone marrow microenvironment in MM is characterized by intricate interactions between malignant plasma cells and various immune cell populations, including T cells, natural killer (NK) cells, macrophages, and dendritic cells [19, 20]. These interactions contribute to immune evasion, tumor proliferation, and drug resistance. Simultaneously, metabolic reprogramming—a hallmark of cancer—has been increasingly recognized in MM, with alterations in glucose metabolism, lipid metabolism, and amino acid utilization facilitating the heightened energetic demands of malignant cells [19, 21]. The convergence of immune dysfunction and metabolic reprogramming, collectively termed immunometabolic dysregulation, represents a promising yet underexplored avenue for prognostic biomarker development. However, most existing prognostic models focus on tumor-intrinsic features (such as cytogenetics and tumor burden) while neglecting these systemic immunometabolic alterations [22, 23]. Recent advances in high-throughput transcriptomic technologies have enabled comprehensive characterization of the molecular landscape of MM [24, 25]. Gene expression profiling (GEP) studies have identified several prognostic signatures, such as the UAMS-70 and EMC92 models, which demonstrate superior capacity to identify high-risk patients compared to conventional staging systems [26, 27]. These signatures capture not only the biology of tumor cells but also features of the tumor microenvironment, including immune cell composition and metabolic pathway activity. However, the clinical translation of these molecular signatures has been hindered by several factors: the requirement for specialized platforms, a lack of standardization, and limited validation in real-world clinical cohorts. Furthermore, the relationship between transcriptomic signatures and readily measurable clinical biomarkers, including peripheral blood counts, serum proteins, and inflammatory markers, remains inadequately characterized. Bridging the gap between molecular findings and routine clinical parameters may facilitate the development of more accessible and practical prognostic tools.

In this study, we employed an integrative analytical strategy to systematically characterize the immunometabolic landscape of MM and to validate its clinical prognostic value. Initially, we analyzed transcriptomic data from the GSE24080 dataset to identify differentially expressed genes (DEGs), elucidate enriched pathways, characterize immune cell infiltration patterns, and develop a robust molecular classifier for MM. Second, we leveraged a well-annotated clinical cohort of 101 newly diagnosed MM patients to investigate the distribution of immunometabolic biomarkers across disease stages, explore correlations between these biomarkers, and evaluate their prognostic significance through survival analysis. By integrating molecular findings with clinical parameters, we aimed to identify clinically accessible biomarkers indicative of the underlying immunometabolic dysregulation in MM and to develop a practical prognostic framework that complements existing staging systems. We hypothesized that specific immunometabolic signatures, particularly those related to tumor burden (β_2-MG) and its systemic consequences (anemia), would demonstrate significant prognostic value and provide insights into the biological mechanisms driving disease progression. Ultimately, this integrative approach might offer new opportunities for risk stratification and personalized therapeutic strategies in MM.

2. MATERIALS AND METHODS

2.1 Study Design and Data Sources

This study utilized an integrative analytical strategy to systematically characterize the immunometabolic landscape of MM and validate its clinical prognostic value through parallel analysis of public transcriptomic datasets and a real-world clinical cohort. The study workflow is illustrated in ***Figure 1***.

2.1.1 GEO Transcriptomic Data

Transcriptomic data were obtained from the GSE24080 dataset in the Gene Expression Omnibus (GEO) database. This dataset contains gene expression profiles from 559 bone marrow samples, including 325 patients with newly diagnosed MM and 234 healthy donors. Raw CEL files were processed using the Robust Multi-array Average (RMA) algorithm for background correction, quantile normalization, and probe summarization. Expression values were $\log_2$-transformed for subsequent analyses.

2.1.2 Clinical Cohort Data

Clinical data were retrospectively collected from patients newly diagnosed with MM at the Department of Hematology of a tertiary hospital between January 2016 and December 2020. The inclusion criteria were as follows: (1) diagnosis meeting the 2014 International Myeloma Working Group (IMWG) criteria; (2) age ≥ 18 years; (3) complete baseline laboratory examinations and survival follow-up data. The exclusion criteria were as follows: (1) presence of concurrent malignancies; (2) active infection or systemic glucocorticoid therapy within 3 months prior to diagnosis; (3) missing > 20% of critical clinical variables. A total of 101 patients were ultimately enrolled.

Baseline data collected included demographic characteristics (age, sex), ISS stages, CRAB criteria, peripheral blood parameters (white blood cell [WBC] count, absolute neutrophil count [ANC] and percentage, hemoglobin [HGB], platelet count [PLT], serum β_2-MG, bone marrow plasma cell percentage (BMPC), serum creatinine,

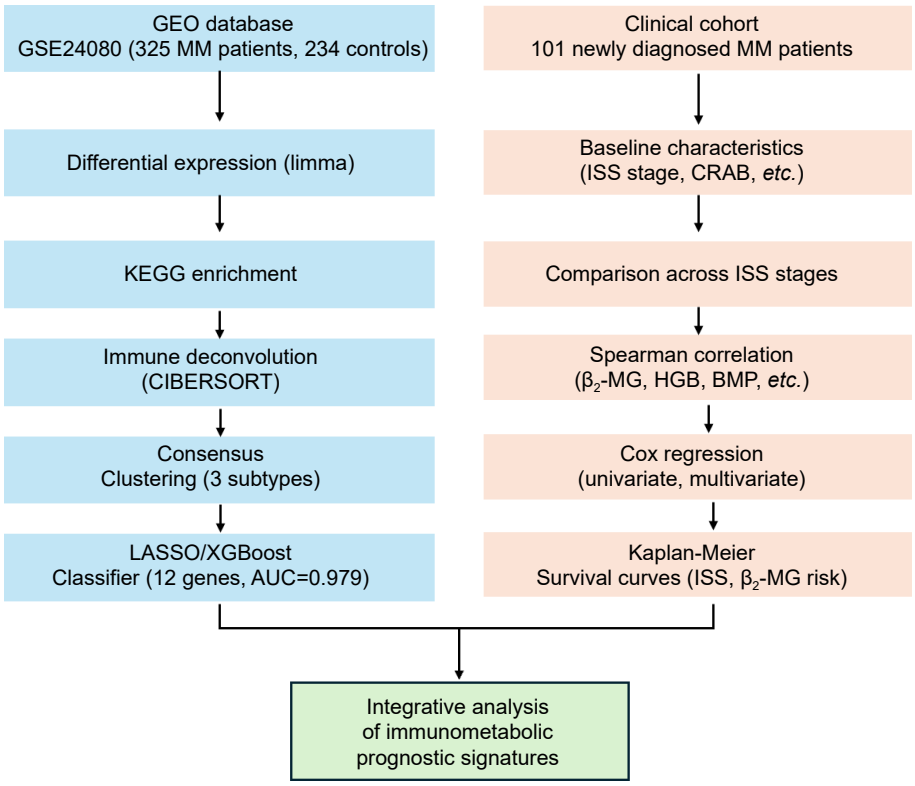

FIGURE 1 Study workflow and integrative analysis strategy. This diagram illustrates the analytical pipeline integrating transcriptomic and clinical data to identify immunometabolic prognostic signatures in multiple myeloma (MM). Left arm (transcriptomic analysis): Publicly available gene expression data from the GSE24080 dataset (325 MM patients, 234 healthy controls) were processed to identify differentially expressed genes (DEGs) using limma, followed by Kyoto Encyclopedia of Genes and Genomes (KEGG) pathway enrichment analysis. Immune cell infiltration was estimated *via* Cell-type Identification By Estimating Relative Subsets Of RNA Transcripts (CIBERSORT). Unsupervised consensus clustering defined three immunometabolic subtypes, and a 12-gene classifier was developed using least absolute shrinkage and selection operator (LASSO) regression (area under the curve [AUC] = 0.979). Right arm (clinical cohort analysis): A retrospective cohort of 101 newly diagnosed MM patients was analyzed for baseline characteristics (including International Staging System [ISS] stages and CRAB features). Comparisons across ISS stages, Spearman correlations among key biomarkers (β_2-microglobulin [β_2-MG], hemoglobin [HGB], bone marrow plasma [BMP] cells), univariate/multivariate Cox regression, and Kaplan-Meier survival analyses were performed. Bottom (integration): Findings from both arms were integrated to identify clinically relevant immunometabolic prognostic signatures, highlighting the independent prognostic value of β_2-MG and HGB and their correlation with tumor burden and hematopoietic suppression. GEO database, Gene Expression Omnibus database.

albumin, lactate dehydrogenase, and 25-hydroxyvitamin D. Survival data were defined as the time interval (months) from diagnosis to all-cause mortality or last follow-up (June 2025); patients lost to follow-up were censored at the date of last contact.

The study was conducted according to the guidelines of the Declaration of Helsinki, and approved by the Ethics Committee of People's Hospital of Ningxia Hui Autonomous Region (Approval No. 2025-WJW-033; date of approval: February 28, 2025). Informed consent was obtained from all subjects involved in the study. Of note, due to the retrospective nature of the study, detailed treatment regimens and cytogenetic data were not available for analysis, which represents a limitation of this clinical cohort.

2.2 GEO Transcriptomic Data Analysis

2.2.1 *Differential Expression and Functional Enrichment Analysis*

The limma package in R was used to identify DEGs between MM patients and healthy controls. Thresholds were set as $|\log_2(\text{fold change, FC})| > 1$ and a false discovery rate (FDR) < 0.05. Kyoto Encyclopedia of Genes and Genomes (KEGG) pathway enrichment analysis was performed using the clusterProfiler package, with an FDR of < 0.05 considered statistically significant.

2.2.2 *Immune Cell Infiltration Analysis*

The Cell-type Identification By Estimating Relative Subsets Of RNA Transcripts (CIBERSORT) algorithm (100 permutations) was applied to estimate the relative abundances of 22 immune cell subsets based on the gene expression matrix. Only samples with a CIBERSORT output *p*-value less than 0.05 were retained to ensure reliable deconvolution. Following filtering, 471 samples (260 MM patients and 211 controls) were retained for immune infiltration analysis. The Wilcoxon rank-sum test was used to compare immune cell proportions between the MM and control groups.

2.2.3 *Molecular Subtype Identification*

An expression matrix was constructed utilizing immunometabolism-

related DEGs. Unsupervised consensus clustering was performed using the package ConsensusClusterPlus with Euclidean distance and Ward's linkage, 1000 iterations, and 80% item resampling. The optimal number of clusters (k = 3) was identified based on the relative change in the area under the cumulative distribution function (CDF) curve (Delta area) and consensus matrix heatmaps.

2.2.4 Feature Gene Selection and Classification Model Construction

To identify immunometabolism-related genes with optimal discriminatory power, least absolute shrinkage and selection operator (LASSO) logistic regression was employed for feature selection. The penalty parameter λ was determined using 10-fold cross-validation, and genes with non-zero coefficients at the minimal cross-validation error were selected. An extreme gradient boosting (XGBoost) model was additionally developed for comparison. Model discrimination was evaluated using the area under the receiver operating characteristic curve (AUC).

2.3 Clinical Cohort Data Analysis

2.3.1 Baseline Characteristics and Intergroup Comparisons

Continuous variables were presented as mean ± standard deviation (SD), while categorical variables were reported as frequencies (percentages). Patients were stratified into three groups according to the ISS: stage I, II, and III. For intergroup comparisons, continuous variables were analyzed using one-way analysis of variance (ANOVA) if normally distributed (as determined by the Shapiro–Wilk test) and homoscedastic (assessed by Levene's test); otherwise, the Kruskal–Wallis rank-sum test was applied. Categorical variables were compared using Pearson's chi-square test or Fisher's exact test. All tests were two-sided, with a significance level of α = 0.05.

2.3.2 Correlation Analysis

Spearman's rank correlation coefficient was used to evaluate the relationships between peripheral blood parameters (WBC count, ANC, neutrophil percentage [Neu%], HGB, PLT) and disease burden indicators (serum β_2-MG, BMPC). Correlation matrices were visualized using heatmaps.

2.3.3 Survival Analysis

OS was defined as the time interval from the date of diagnosis to the date of death from any cause or last follow-up, censoring patients who were lost to follow-up at their last known contact. Survival durations were recorded in months. Initially, univariate Cox proportional hazards regression analysis was performed to evaluate the association of each potential prognostic factor with OS. The variables included in the analysis were age, sex, WBC count, Neu%, serum β_2-MG, BMPC, HGB, and PLT. Hazard ratios (HRs) and 95% confidence intervals (CIs) were calculated. Variables with a p-value < 0.05 in the univariate analysis were subsequently entered into a multivariate Cox proportional hazards model to identify independent prognostic factors. A backward stepwise selection procedure based on the Akaike information criterion (AIC) was applied to retain the most parsimonious set of predictors. The proportional hazards assumption for each variable was verified through examination of the scaled Schoenfeld residuals and graphical assessment of log-minus-log plots; no violations were detected. Results were visualized using forest plots, with statistical significance established at a two-tailed α level of 0.05. All analyses were performed using R software (version 4.1.0; R Foundation for Statistical Computing, Vienna, Austria) with the survival package.

3. RESULTS

3.1 Differential Gene Expression, Functional Enrichment, and Co-Expression Networks in MM

DEGs were identified between 325 MM cases and 234 controls in the GSE24080 dataset using the limma package. As shown in ***Figure 2A***, the volcano plot separates upregulated and downregulated transcripts under the criteria of an adjusted p < 0.05 and $|\log_2(FC)| > 1$, yielding 342 upregulated and 112 downregulated DEGs. The heatmap presented in ***Figure 2B*** displays the top 40 DEGs, highlighting distinct expression profiles between MM and control samples, with genes such as *MT1M*,

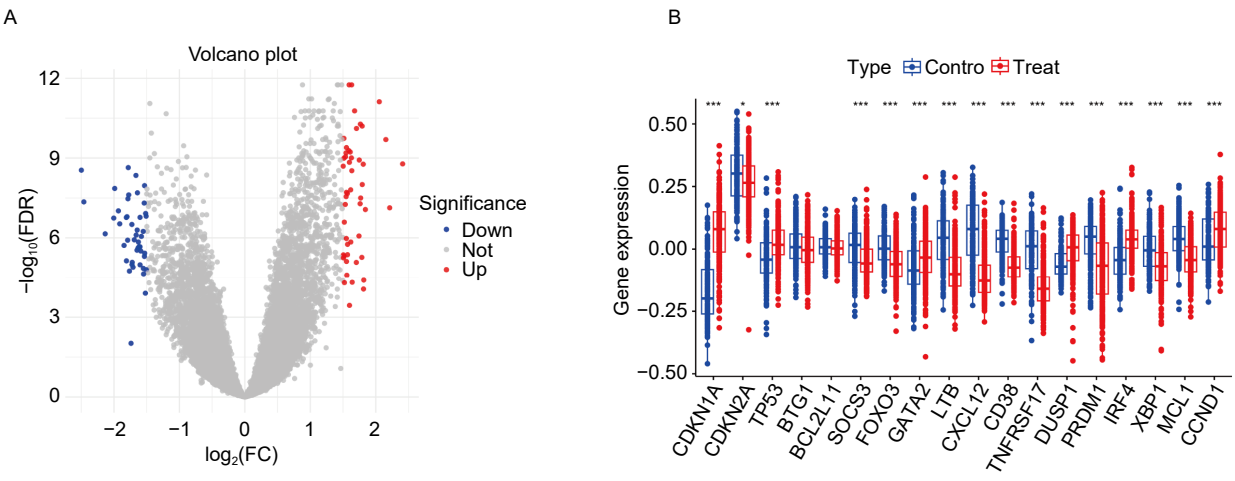

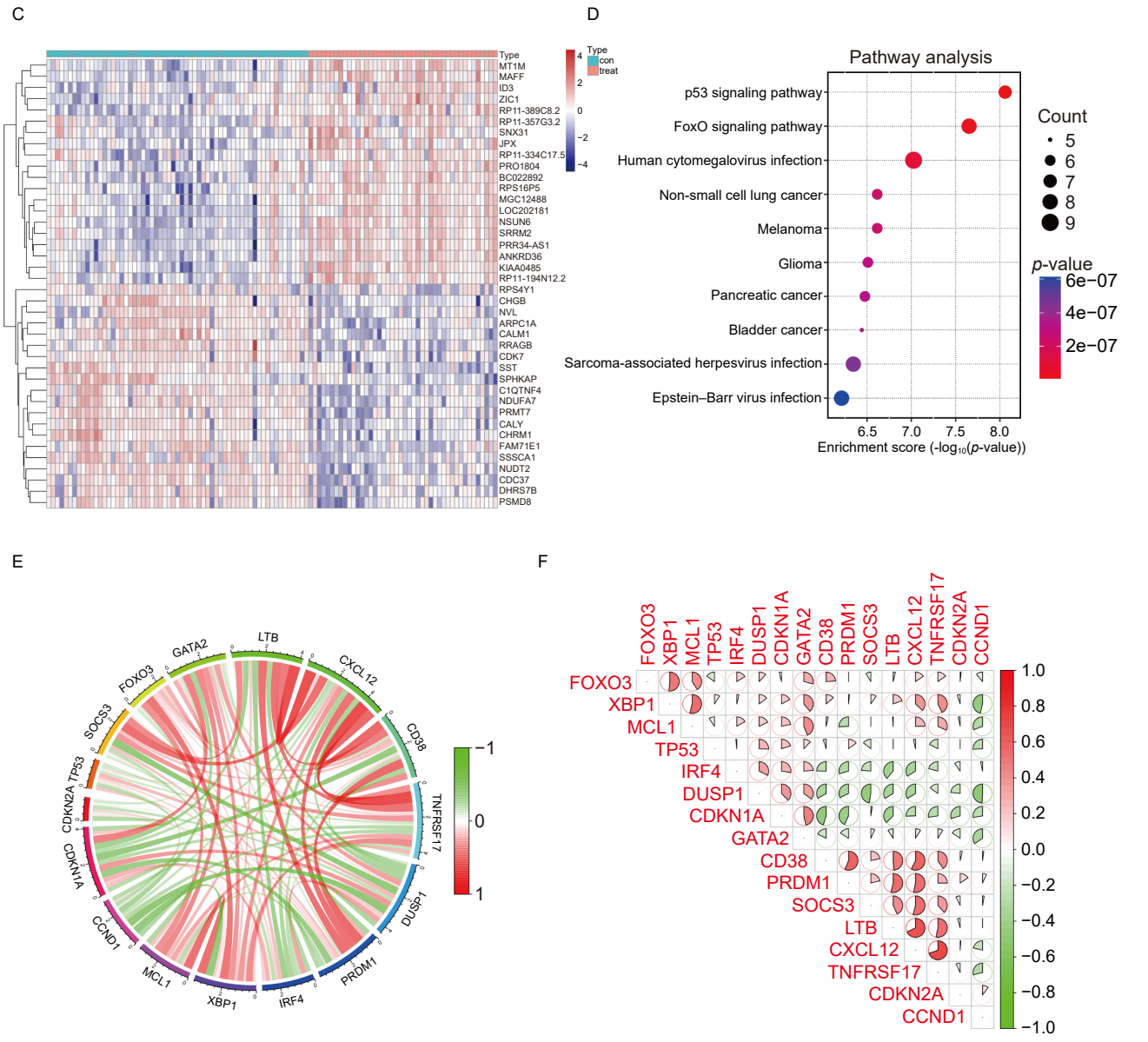

FIGURE 2 Differential gene expression, functional enrichment, and co-expression networks in multiple myeloma (MM). (A) Volcano plot showing differentially expressed genes (DEGs) between MM patients and healthy controls. Red and blue dots represent significantly upregulated and downregulated genes, respectively ($|\log_2(\text{fold change, FC})| > 1$, false discovery rate (FDR) < 0.05). (B) Heatmap of the top 40 DEGs, demonstrating distinct expression patterns between MM and control samples. (C) Boxplots of selected DEGs showing significant dysregulation in MM, including *CDKN1A*, *CDKN2A*, *TP53*, *SOCS3*, *FOXO3*, and *IRF4*. (D) KEGG pathway enrichment analysis of DEGs, highlighting significant enrichment in p53 signaling, FOXO signaling, and infection-related pathways. (E) Circos plot illustrating co-expression relationships among key immunometabolic genes; red lines indicate positive correlations, green lines indicate negative correlations, with line width proportional to correlation strength. (F) Spearman correlation matrix of hub immunometabolic genes, with color intensity representing correlation strength. Asterisks denote statistical significance (*$p < 0.05$, **$p < 0.01$, ***$p < 0.001$).

MAFF, *ID3*, *ZIC1*, *CALM1*, and *PSMD8* showing pronounced differences. Boxplot comparisons of representative DEGs (***Figure 2C***) revealed significant dysregulation of *CDKN1A*, *CDKN2A*, *TP53*, *SOCS3*, *FOXO3*, and *IRF4* in MM compared to controls.

To elucidate the biological functions underlying these transcriptional alterations, KEGG enrichment analysis was performed. The results indicated that DEGs were predominantly enriched in the p53 signaling pathway, the FOXO signaling pathway, and infection-related pathways (***Figure 2D***). These pathways are critically involved in cell cycle regulation, apoptosis, metabolism, and immune responses, suggesting their potential roles in MM pathogenesis.

To examine the coordination among these immunometabolic transcripts, we conducted a co-expression network analysis. The Circos plot (***Figure 2E***) depicts positive (red) and negative (green) correlations among key DEGs, with link width proportional to

correlation strength. Among these, *CXCL2* exhibited a positive correlation with *SOCS3* and *TNFRSF17*, whereas *CDKN1A* showed a negative correlation with *CD38* and *PRDM1*. The correlation matrix (***Figure 2F***) further revealed significant positive correlations between *CDKN1A* and *GATA2*, *CD38* and *PRDM1*, and *CXCL12* and *TNFRSF17*, alongside negative correlations between *CDKN1A* and *CD38*, *DUSP1* and *CCND1*, and *XBP1* and *CCND1*. These findings indicate a coordinated dysregulation of immunometabolic gene networks in MM.

3.2 Immune Cell Infiltration Landscape and Gene-Cell Interactions

Given the enrichment of immune-related pathways and the identification of immunometabolic hub genes, we subsequently characterized the tumor immune microenvironment in MM. The application of the CIBERSORT algorithm to estimate the relative proportions of 22 immune cell types from the GSE24080 expression profiles revealed a markedly altered immune cell composition in MM samples compared to healthy controls (***Figure 3A***). Specifically, naive B cells, memory B cells, $CD8^+$ T cells, $CD4^+$ naive T cells, and activated NK cells were significantly decreased in MM, whereas plasma cells, $CD4^+$ memory-activated T cells, regulatory T cells (Tregs), monocytes, M0 macrophages, M2 macrophages, and activated dendritic cells were notably enriched (Wilcoxon test, $p < 0.05$).

To explore potential regulatory relationships, we examined the correlations between hub immunometabolic genes and infiltrating immune cell populations. The Spearman correlation heatmap (***Figure 3B***) revealed distinct association patterns: *GATA2* was positively correlated with plasma cells and Tregs but negatively correlated with naive B cells and $CD8^+$ T cells; *CXCL12* showed positive correlations with naive B cells and $CD8^+$ T cells, and negative correlations with monocytes and M0 macrophages; *IRF4* was positively correlated with M2 macrophages, Tregs, and plasma cells; *TP53* displayed positive associations with activated dendritic cells and negative associations with M0 macrophages. These findings underscore specific gene–immune cell interaction networks potentially involved in MM pathogenesis and immune evasion.

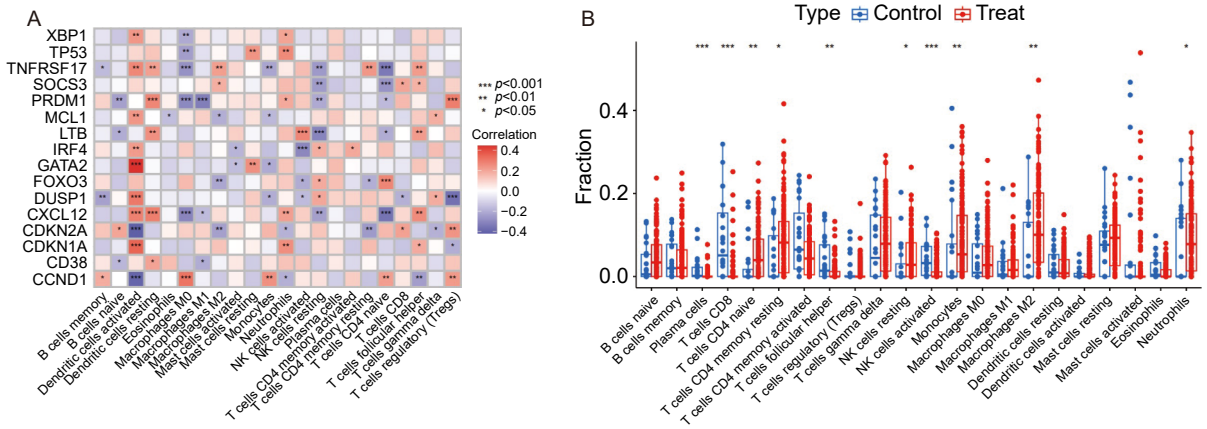

FIGURE 3 Immune cell infiltration and gene-cell interactions in multiple myeloma (MM). (A) Boxplots comparing the relative proportions of 22 immune cell subsets estimated by CIBERSORT between MM patients and healthy controls. Naive B cells, memory B cells, $CD8^+$ T cells, $CD4^+$ naive T cells, and activated natural killer (NK) cells were significantly decreased in MM, whereas plasma cells, $CD4^+$ memory activated T cells, regulatory T cells (Tregs), monocytes, M0 macrophages, M2 macrophages, and activated dendritic cells were significantly enriched (Wilcoxon test, $p < 0.05$). (B) Spearman correlation heatmap showing relationships between hub immunometabolic genes and infiltrating immune cell populations. Color intensity represents correlation strength, with red indicating positive correlations and blue indicating negative correlations. Asterisks denote statistical significance (*$p < 0.05$, **$p < 0.01$, ***$p < 0.001$).

3.3 Molecular Subtype Identification and Transcriptomic Classifier Performance

The observed heterogeneity in both gene expression and immune infiltration prompted an investigation into whether immunometabolic gene signatures could define distinct molecular subtypes. Unsupervised consensus clustering of immunometabolic DEGs was performed using the ConsensusClusterPlus algorithm. To determine the optimal number of clusters, we evaluated the CDF curves across different k values (***Figure 4B***). The CDF curves became progressively smoother as k increased, with the most significant improvement occurring at $k = 3$. The Delta area plot (***Figure 4C***) further confirmed that additional clusters beyond $k = 3$ contributed only marginally to the CDF area, indicating that $k = 3$ provided the most robust representation of molecular subtypes. The consensus matrix heatmap for $k = 3$ (***Figure 4A***) demonstrated distinct separation and high intra-cluster consistency, supporting the presence of three distinct immunometabolic subtypes among MM patients.

Based on the identified molecular subtypes and hub genes, we sought to develop a robust classifier for MM detection. LASSO logistic regression was applied to identify the most discriminative immunometabolic genes, yielding a 12-gene signature with minimal classification error across cross-validation folds (***Figure 4D***). The 12 genes identified were *CDKN1A*, *CDKN2A*, *SOCS3*, *GATA2*,

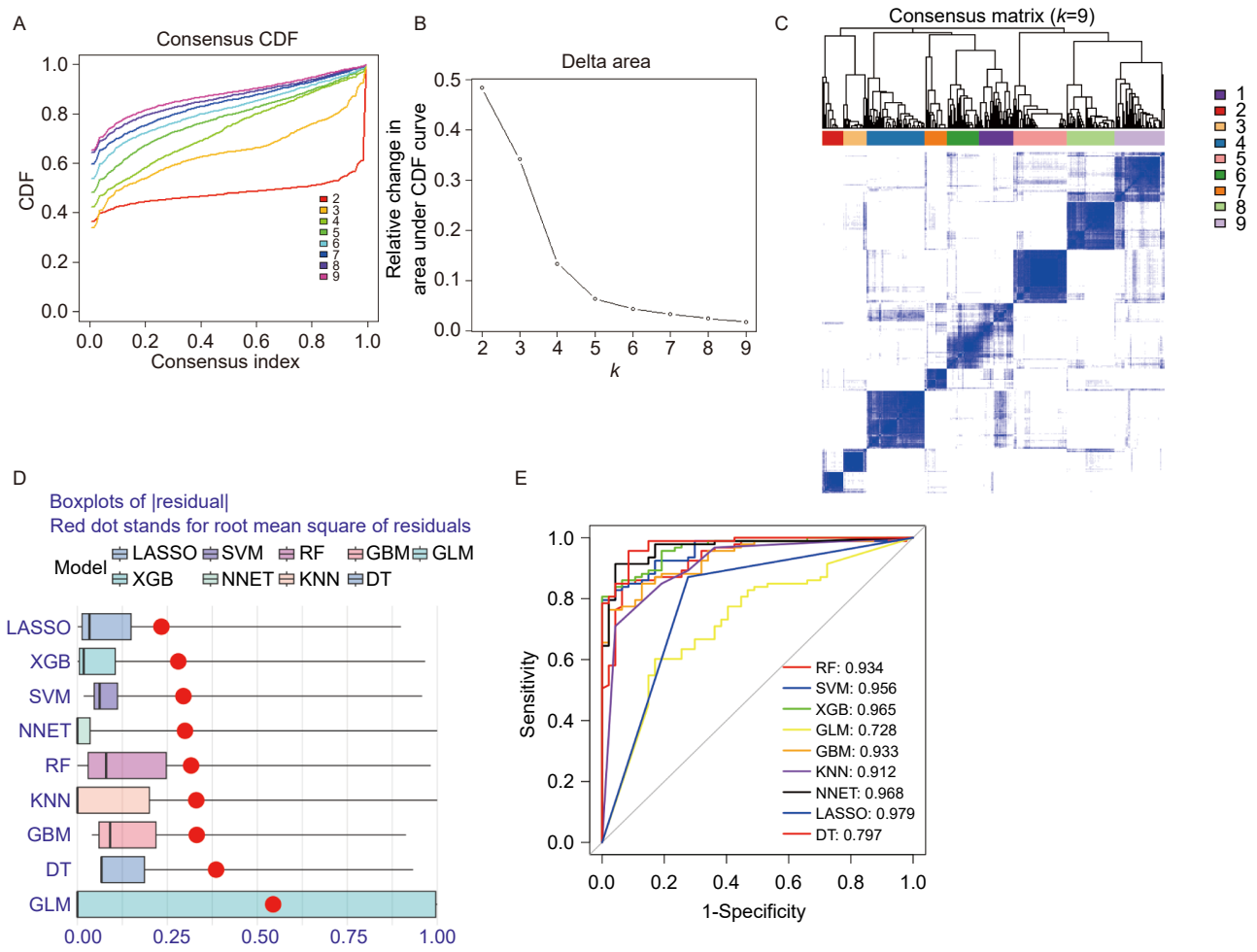

FIGURE 4 Molecular subtype identification and transcriptomic classifier performance. (A) Consensus matrix heatmap for k = 3, demonstrating clear separation and high intra-cluster consistency among three distinct immunometabolic subtypes in multiple myeloma (MM) patients. (B) Cumulative distribution function (CDF) curves for k = 2 to 9, illustrating the relative stability of clustering solutions. (C) Delta area plot showing the relative change in the area under the CDF curve; the optimal number of clusters is indicated at k = 3, where additional clusters contribute only marginally to clustering improvement. (D) LASSO regression cross-validation error curve. The optimal log(λ) value corresponding to the 12-gene signature (*CDKN1A*, *CDKN2A*, *SOCS3*, *GATA2*, *XBP1*, *CXCL12*, *CD38*, *TNFRSF17*, *DUSP1*, *PRDM1*, *IRF4*, *CCND1*) is marked by the vertical dashed line, with minimal classification error across ten-fold cross-validation. (E) Receiver operating characteristic (ROC) curve for the least absolute shrinkage and selection operator (LASSO) classifier, achieving an area under the curve (AUC) of 0.979, indicating excellent discriminatory performance for distinguishing MM cases from controls.

XBP1, *CXCL12*, *CD38*, *TNFRSF17*, *DUSP1*, *PRDM1*, *IRF4*, and *CCND1*. An XGBoost model was also trained for comparison. The LASSO classifier demonstrated outstanding discriminative performance, achieving an AUC of 0.979 (***Figure 4E***), which reflects its high sensitivity and specificity in differentiating MM cases from controls. This 12-gene signature represents a parsimonious yet powerful tool for the molecular classification of MM, capturing the principal immunometabolic dysregulations identified in our preceding analyses.

3.4 Baseline Characteristics of the Clinical Cohort

To validate the clinical relevance of these molecular findings, we analyzed a cohort of 101 patients newly diagnosed with MM. ***Table 1*** presents a summary of the baseline demographic and clinical characteristics. The mean age of the cohort was 63.2 years (SD = 9.6), with a male predominance (60%). Of the 101 patients in total, 16 had missing albumin or β_2-MG data that precluded ISS staging calculation; thus, the stage-stratified analysis was performed on the remaining 85 patients with complete staging data. According to the ISS, 14 patients (13.9%) were classified as Stage I, 35 (34.6%) as Stage II, and 36 (35.6%) as Stage III. The majority of patients (67.5%) presented with at least one CRAB feature. The mean WBC count was 5.96 × 10^3/μL (SD = 3.37), and the mean serum β_2-MG level was 7.2 mg/L (SD = 7.3), with 41.7% of patients classified as high-risk (β_2-MG > 5.5 mg/L). The mean BMPC was 19.5% (SD = 23.1). Over a median follow-up period of 27.9 months, 37 deaths were recorded, yielding a mortality rate of 36.6%.

TABLE 1 Baseline characteristics of newly diagnosed MM patients stratified by ISS stages

Characteristic	Total (n = 101)	ISS Stage I[j] (n = 14)	ISS Stage II[k] (n = 35)	ISS Stage III[l] (n = 36)	p-value
Age, years, mean (SD)	63.2 (9.6)	61.43 (12.28)	63.29 (8.81)	63.86 (9.41)	0.728
Male [n (%)]	60 (59.4)	7 (50.0)	24 (68.6)	20 (55.6)	0.377
CRAB features present [n (%)]	56 (67.5)[a]	3 (23.1)	24 (70.6)	29 (80.6)	**0.001**
Bone marrow plasma cells (%), mean (SD)	19.5 (23.1)	10.15 (9.10)	13.35 (18.17)	28.41 (27.51)	**0.006**
HGB (g/L), mean (SD)	103.0 (30.2)[b]	128.50 (26.49)	122.60 (25.73)	84.61 (21.50)	**<0.001**
Anemia [n (%)]	60 (59.4)	6 (42.9)	20 (57.1)	34 (94.4)	**<0.001**
WBC count (×10³/μL), mean (SD)	5.96 (3.37)	6.41 (3.84)	6.18 (3.35)	5.58 (3.26)	0.656
Neu% (%), mean (SD)	59.8 (14.2)[c]	65.68 (12.15)	55.25 (15.38)	61.57 (13.20)	**0.039**
PLT (×10³/μL), mean (SD)	185.1 (94.7)[d]	220.71 (64.03)	188.97 (96.16)	167.54 (101.02)	0.199
Serum β_2-MG (mg/L), mean (SD)	7.20 (7.29)	2.44 (0.46)	3.52 (1.42)	12.64 (8.51)	**<0.001**
β_2-MG risk stratification [n (%)[i]]					**<0.001**
Low (≤ 3.5 mg/L)	33 (39.3)	14 (100.0)	19 (54.3)	0 (0.0)	-
Intermediate (3.5–5.5 mg/L)	16 (19.0)	0 (0.0)	15 (42.9)	1 (2.9)	-
High (> 5.5 mg/L)	35 (41.7)	0 (0.0)	1 (2.9)	34 (97.1)	-
Serum creatinine (μmol/L), mean (SD)	158.2 (171.3)[e]	57.67 (18.32)	70.31 (23.12)	264.71 (230.42)	**<0.001**
Albumin (g/L), mean (SD)	31.2 (7.1)[f]	37.16 (2.01)	29.29 (7.55)	29.63 (6.35)	**<0.001**
25-hydroxyvitamin D (ng/mL), mean (SD)	19.8 (13.2)[g]	34.91 (22.02)	16.93 (9.10)	16.36 (7.93)	**0.013**
Survival time (months), mean (SD)	30.8 (13.4)[h]	46.39 (3.18)	34.67 (10.78)	19.64 (7.07)	**<0.001**
Death events [n (%)]	37 (36.6)	1 (7.1)	11 (31.4)	25 (69.4)	**<0.001**

The p values were derived from ANOVA or Kruskal-Wallis test for continuous variables and chi-square test for categorical variables, as appropriate. Bold font indicates statistical significance ($p < 0.05$). [a] Based on 83 patients with available CRAB data. [b] Calculated from ***Table 1*** data (mean of stage-specific means weighted by sample size). [c-h] Calculated from stage-specific means. [i] Data for β_2-MG and its risk stratification were available for 84 patients. [j-l] ISS stage data were available for 85 patients (14 Stage I, 35 Stage II, 36 Stage III). MM, multiple myeloma; ISS, International Staging System; SD, standard deviation; CRAB, hypercalcemia, renal insufficiency, anemia, bone lesions; HGB, hemoglobin; WBC, white blood cell; Neu%, neutrophil percentage; PLT, platelet count; β_2-MG, β_2-microglobulin.

3.5 Clinical Characteristics Across ISS Stages

When stratified by ISS, significant differences in clinical and laboratory parameters were observed across the three stages (***Table 1***). As expected, patients diagnosed with Stage III disease exhibited the most aggressive clinical features. The proportion of patients presenting with CRAB features increased significantly from Stage I (23.1%) to Stage III (80.6%, $p = 0.001$). Consistent with the ISS definition, β_2-MG levels were markedly higher in Stage III patients (mean 12.64 mg/L) relative to those in Stage I (2.44 mg/L) and Stage II (3.52 mg/L, $p < 0.001$).

Additional indicators of disease burden also showed significant differences. HGB levels were dramatically lower in Stage III patients (mean 84.61 g/L) compared to those in Stage I (128.50 g/L) and Stage II (122.60 g/L) patients ($p < 0.001$), indicating more severe anemia—a clinical manifestation that aligns with the erythroid suppression suggested by our transcriptomic findings. The BMPC was also highest in the Stage III group (mean 28.41%, $p = 0.006$). Notably, the percentage of neutrophils exhibited significant variation among the groups ($p = 0.039$), while the total WBC count did not ($p = 0.3925$), as confirmed by ANOVA and Kruskal-Wallis tests. Consequently, survival outcomes were significantly poorer for Stage III patients, with a mean survival time of only 19.6 months compared to 46.4 months for Stage I and 34.7 months for Stage II ($p < 0.001$).

3.6 Correlation Among Clinical Biomarkers

To explore the interrelationships between key clinical biomarkers, we performed a Spearman correlation analysis, visualized as a heatmap in ***Figure 5A***. A strong positive correlation was observed between WBC count and ANC (Spearman's $\rho = 0.93$, $p < 0.001$), which is biologically expected.

More importantly, we identified significant correlations between indicators of tumor burden and systemic effects. As shown in ***Figure 5B***, serum β_2-MG, a key indicator of tumor load, exhibited a strong negative correlation with HGB levels ($\rho = -0.70$, $p < 0.001$), confirming the association between disease progression and the development of anemia—a finding that resonates with the dysregulated erythropoiesis-related pathways identified in our transcriptomic analysis. β_2-MG also demonstrated a moderate positive correlation with BMPC ($\rho = 0.43$, $p < 0.001$), as illustrated in the heatmap (***Figure 5A***). Conversely, BMPC was negatively correlated with both HGB ($\rho = -0.48$, $p < 0.001$) and WBC count

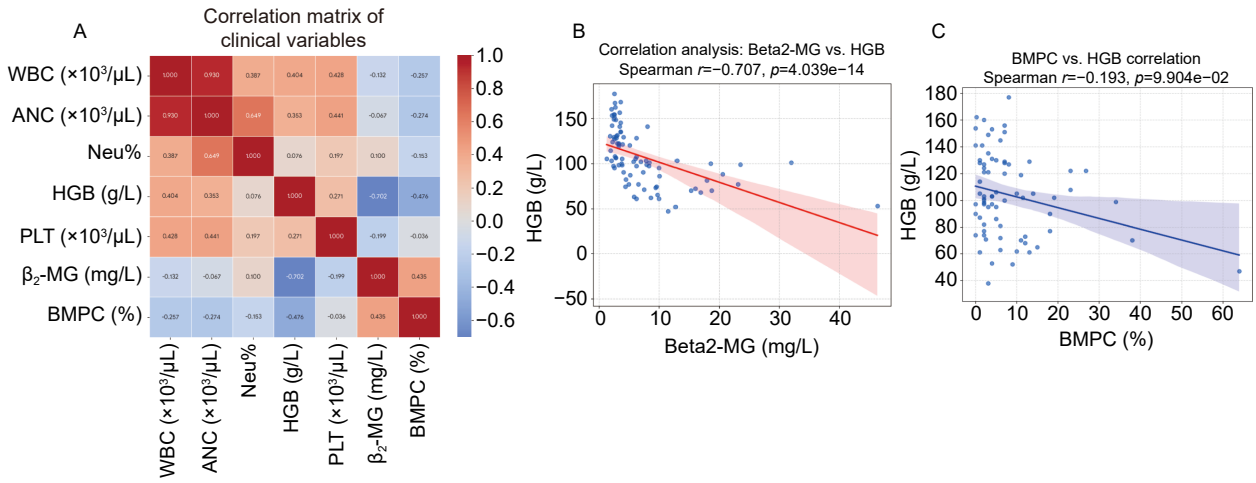

FIGURE 5 Correlation analysis of clinical biomarkers in multiple myeloma (MM). (A) Heatmap of Spearman correlation coefficients among peripheral blood parameters and disease burden indicators, including white blood cell (WBC) count, absolute neutrophil count (ANC), neutrophil percentage (Neu%), hemoglobin (HGB), platelet count (PLT), serum β_2-microglobulin (β_2-MG), and bone marrow plasma cell percentage (BMPC). Color intensity represents correlation strength, with red indicating positive correlations and blue indicating negative correlations. Asterisks denote statistical significance (*p < 0.05, **p < 0.01, ***p < 0.001). (B) Scatter plot showing the strong negative correlation between serum β_2-MG and HGB levels (Spearman's ρ = −0.70, p < 0.001). The blue line represents the linear regression line with 95% confidence interval (CI) (gray shading), directly visualizing the relationship between tumor burden and anemia. (C) Scatter plot showing the negative correlation between BMPC and HGB levels (Spearman's ρ = −0.48, p < 0.001), with linear regression line and 95% CI. This finding supports the concept that extensive bone marrow infiltration suppresses normal hematopoietic function.

(ρ = −0.26, p = 0.008). ***Figure 5C*** further illustrates the negative correlation between BMPC and HGB levels. These findings suggest that extensive bone marrow infiltration may suppress normal hematopoietic function, consistent with the altered immune cell composition observed in the GEO analysis.

3.7 Prognostic Factors for OS

To identify predictors of survival, we performed univariate and multivariate Cox proportional hazards regression analyses. In the univariate analysis (***Table 2***), several factors were significantly associated with OS. Older age at diagnosis was identified as a significant risk factor (HR = 1.046, 95% CI: 1.012–1.081, p = 0.0069). Elevated levels of classic tumor burden markers, namely serum β_2-MG (HR = 1.098, 95% CI: 1.062–1.135, p < 0.001) and BMPC (HR = 1.022, 95% CI: 1.010–1.035, p < 0.001), were associated with a significantly increased risk of mortality. Conversely, elevated HGB (HR = 0.966, 95% CI: 0.953–0.979, p < 0.001) and PLT (HR = 0.994, 95% CI: 0.990–0.999, p = 0.0087) were identified as protective factors, with higher levels correlating with improved survival.

Variables that were significant in the univariate analysis (p < 0.05) were subsequently included in the multivariate Cox regression model. The forest plot in ***Figure 6C*** visually summarizes the independent prognostic factors identified through multivariate analysis. After adjusting for confounders, three factors retained their independent prognostic significance. Age remained an independent predictor, with older patients exhibiting a poorer prognosis (HR = 1.041, 95% CI: 1.004–1.079, p = 0.029). Serum β_2-MG emerged as the strongest independent risk factor; for each one-unit increase in β_2-MG, the risk of death increased by 6.5% (HR = 1.065, 95% CI: 1.022–1.110, p = 0.0027). HGB level remained an independent protective factor, with higher HGB associated with a reduced risk of mortality (HR = 0.978, 95% CI: 0.962–0.994, p = 0.0089). BMPC and PLT, significant in univariate analysis, did not demonstrate independent prognostic value in the multivariate model, suggesting their effects may be mediated through or confounded by stronger predictors such as β_2-MG and HGB.

To further visualize the prognostic impact of key risk stratification systems, we performed Kaplan-Meier survival analysis. As shown in ***Figure 6A***, patients stratified by ISS

TABLE 2 Univariate Cox regression analysis of OS in MM patients

Variable	HR	95% CI	p-value
Age	1.046	1.012-1.081	**0.0069**
Sex (male vs. female)	1.195	0.618-2.312	0.5971
WBC count	0.932	0.831-1.045	0.2289
Neu%	1.004	0.981-1.027	0.7377
Serum β_2-MG	1.098	1.062-1.135	**< 0.001**
BMPC	1.022	1.010-1.035	**< 0.001**
HGB	0.966	0.953-0.979	**< 0.001**
PLT	0.994	0.990-0.999	**0.0087**

Bold font indicates statistical significance (p < 0.05). OS, overall survival; MM, multiple myeloma; HR, hazard ratio; CI, confidence interval; WBC, white blood cell; Neu%, neutrophil percentage; β_2-MG, β_2-microglobulin; WBC, white blood cell; BMPC, bone marrow plasma cell percentage; HGB, hemoglobin; PLT, platelet count.

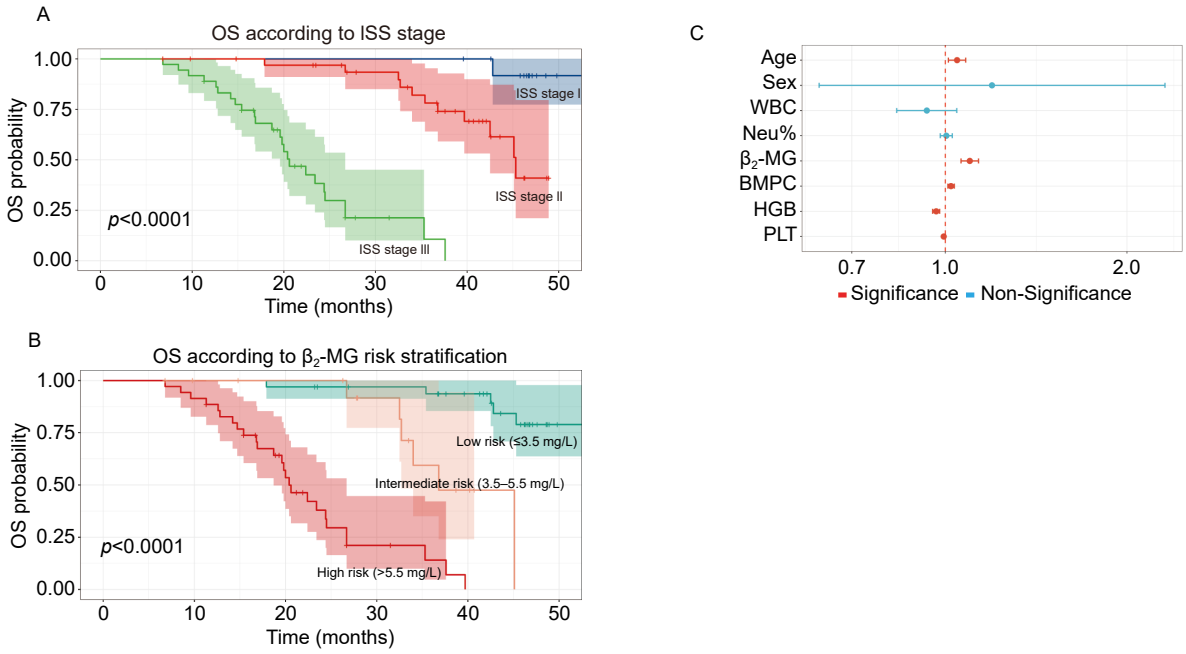

FIGURE 6 Kaplan-Meier survival curves and forest plot for prognostic factors. (A) Overall survival (OS) according to International Staging System (ISS) stages. Patients with stage III disease exhibited significantly worse outcomes compared to those with stages I and II, with median survival times of 46.4 months (stage I), 34.7 months (stage II), and 19.6 months (stage III) (log-rank $p < 0.001$). Tick marks indicate censored patients. (B) OS according to serum β_2-microglobulin (β_2-MG) risk stratification. Patients were categorized as low risk (≤ 3.5 mg/L), intermediate risk (3.5–5.5 mg/L), and high risk (> 5.5 mg/L). Survival differences among the three groups were statistically significant (log-rank $p < 0.001$), with high-risk patients demonstrating the poorest prognosis. (C) Forest plot summarizing independent prognostic factors identified by multivariate Cox regression analysis. Squares represent hazard ratios (HRs), horizontal lines indicate 95% confidence intervals (CI), and the vertical dashed line corresponds to HR = 1. Variables with HR > 1 are risk factors, while those with HR < 1 are protective factors. Age (HR = 1.041, 95% CI: 1.004–1.079, $p = 0.029$), β_2-MG (HR = 1.065, 95% CI: 1.022–1.110, $p = 0.0027$), and hemoglobin (HGB) (HR = 0.978, 95% CI: 0.962–0.994, $p = 0.0089$) retained independent prognostic significance. Asterisks denote statistical significance (*$p < 0.05$, **$p < 0.01$). WBC, white blood cell; Neu%, neutrophil percentage; BMPC, bone marrow plasma cell percentage; PLT, platelet count.

exhibited progressively poorer survival with advancing stage, with median survival time declining from 46.4 months in stage I to 34.7 months in stage II, and 19.6 months in stage III (log-rank $p < 0.001$). Given that serum β_2-MG was the strongest independent risk factor in the multivariate analysis, patients were stratified based on β_2-MG risk categories (low: ≤ 3.5 mg/L; intermediate: 3.5–5.5 mg/L; high: > 5.5 mg/L). The Kaplan-Meier curves (***Figure 6B***) demonstrated a clear separation in survival outcomes across the three risk groups (log-rank $p < 0.001$), with high-risk patients exhibiting the poorest prognosis. These clinical findings provide critical validation for the molecular signatures identified in our GEO analysis, particularly highlighting the central role of tumor burden (β_2-MG) and its systemic hematopoietic consequences (anemia) in determining patient outcomes.

4. DISCUSSION

In this integrative study, we systematically characterized the immunometabolic landscape of MM through parallel analysis of transcriptomic data and a real-world clinical cohort, identifying robust prognostic signatures at both molecular and clinical levels. Our findings reveal that MM is characterized by the coordinated dysregulation of immunometabolic gene networks, profound alterations in immune cell composition, and clinically accessible biomarkers that independently predict patient survival. The convergence of transcriptomic findings with clinical parameters—particularly the strong prognostic value of β_2-MG and HGB, and their correlation with bone marrow plasma cell infiltration—underscores the central role of tumor burden and its systemic hematopoietic consequences in determining patient outcomes.

The transcriptomic analysis revealed 342 upregulated and 112 downregulated genes in MM, with significant enrichment in the p53 and FOXO signaling pathways. The p53 pathway, a critical tumor suppressor mechanism regulating cell cycle arrest and apoptosis, is frequently inactivated in MM through deletion or mutation, leading to impaired apoptosis and chemotherapy resistance [28]. Our finding that *TP53* expression correlates positively with activated dendritic cells and negatively with M0 macrophages suggests that p53 dysfunction may contribute to immune evasion by altering the composition of antigen-presenting cells in the tumor

microenvironment. Similarly, the FOXO pathway, often suppressed by constitutive phosphatidylinositol 3-kinase (PI3K)/AKT signaling in MM, plays a pivotal role in regulating cellular metabolism, oxidative stress, and survival [29]. The enrichment of FOXO signaling among DEGs aligns with previous reports that FOXO inhibition promotes enhanced glycolysis and contributes to metabolic reprogramming in malignant plasma cells [30]. The co-expression networks identified in our analysis, including correlations between *CXCL2* and *SOCS3* as well as between *CDKN1A* and *GATA2*, suggest coordinated dysregulation of genes involved in immune regulation and cell cycle control, highlighting potential nodes for therapeutic intervention.

The immune infiltration analysis revealed a markedly altered bone marrow microenvironment in MM, characterized by a depletion of protective immune populations—including naive B cells, memory B cells, and $CD8^+$ T cells—and an enrichment of immunosuppressive and tumor-promoting populations, such as Tregs, monocytes, and M0/M2 macrophages. This immunological profile is consistent with the established concept of MM-induced immune evasion and dysfunction [31, 32]. Tregs, which suppress effector T cell responses, have been shown to accumulate in the bone marrow of MM patients and correlate with disease progression [33, 34]. Tumor-associated macrophages, particularly M2-polarized macrophages, facilitate angiogenesis, suppress antitumor immunity, and support plasma cell survival through secretion of interleukin-6 (IL-6) and other growth factors [35]. The positive correlation between *IRF4*—a master regulator of plasma cell differentiation and survival—and M2 macrophages observed in our analysis further supports the existence of reciprocal interactions between malignant plasma cells and their supportive microenvironment [36, 37]. The CXCL12/CXCR4 axis recruits immunosuppressive macrophages and Tregs to create an immune-suppressive microenvironment that suppresses $CD8^+$ T-cell cytotoxicity [38]. This process promotes tumor cell homing to bone marrow niches and impairs CAR-T cell infiltration and targeting, resulting in attenuated T-cell-mediated antitumor immunity and cellular therapy resistance [39]. These findings reinforce the notion that therapeutic strategies targeting not only the malignant clone but also the immune microenvironment may enhance treatment efficacy in MM.

The identification of three distinct immunometabolic subtypes through consensus clustering highlights the molecular heterogeneity of MM and suggests that patients may be stratified based on underlying biological differences. Such stratification could inform personalized therapeutic approaches; for example, patients with subtypes characterized by high Treg infiltration may benefit from immunomodulatory agents that target Treg function, while those with metabolic pathway enrichment might respond to metabolic inhibitors. The development of a 12-gene LASSO classifier with excellent diagnostic performance (AUC = 0.979) demonstrates the feasibility of translating these molecular insights into clinically applicable tools. This parsimonious signature, capturing key immunometabolic dysregulations, could complement existing cytogenetic and clinical staging systems to improve risk stratification. Future research should validate this signature in independent cohorts and prospectively assess its utility in guiding treatment decisions. Although our 12-gene LASSO classifier demonstrated excellent diagnostic performance in the transcriptomic dataset, its expression in relation to clinical outcomes could not be validated in our clinical cohort due to the lack of corresponding gene expression data. Future prospective studies should evaluate the prognostic value of this signature using targeted expression assays.

The clinical cohort analysis provides important validation of the molecular findings and identifies readily accessible biomarkers with independent prognostic value. The strong correlation between ISS stage and established markers of disease burden—β_2-MG, HGB, and BMPC—confirms the clinical validity of our cohort and aligns with the known biology of MM progression. The striking inverse correlation between β_2-MG and HGB ($\rho = -0.70$, $p < 0.001$) is particularly noteworthy, as it directly visualizes the relationship between tumor burden and its systemic hematopoietic consequences. β_2-MG, a component of the MHC class I molecule, is shed from the surface of malignant plasma cells and serves as a reliable indicator of tumor mass [40]. HGB reflects the cumulative effects of bone marrow infiltration by malignant plasma cells, the suppression of erythropoiesis by inflammatory cytokines such as IL-6, and renal dysfunction—all common features of advanced MM [41, 42]. The persistence of both β_2-MG and HGB as independent prognostic factors in the multivariate analysis, contrasted with the loss of significance of BMPC and PLT, suggests that these peripheral blood biomarkers may capture not only tumor burden but also the systemic impact of the disease more comprehensively than a single measurement of marrow infiltration. This finding implies that the prognostic effects of bone marrow infiltration and PLT are likely mediated through or confounded by stronger predictors, particularly β_2-MG and HGB.

The negative correlation between BMPC and both HGB and WBC count ($\rho = -0.48$ and -0.26, respectively) supports the concept of hematopoietic suppression mediated by extensive marrow infiltration. This finding resonates with the immune cell alterations observed in our transcriptomic analysis, where MM samples exhibited depletion of multiple hematopoietic lineages, including B cells and T cells. The displacement of normal hematopoietic precursors by malignant plasma cells, combined with the suppressive effects of inflammatory cytokines and alterations in the bone marrow niche, contributes to the cytopenias commonly observed in MM patients [43, 44]. These cytopenias, in turn, heighten susceptibility to infections and limit tolerance to cytotoxic therapies, directly impacting patient outcomes. The survival analyses provide compelling evidence for the prognostic value of both established staging systems and specific immunometabolic biomarkers. The distinct separation of survival curves by ISS stage (log-rank $p < 0.001$) confirms the

continued relevance of this staging system in contemporary practice, while the equally robust stratification by β_2-MG risk categories underscores the central role of this biomarker in MM prognostication. Importantly, the identification of HGB as an independent protective factor—with each 1 g/L increase associated with a 2.2% reduction in mortality risk—highlights the clinical significance of managing anemia in MM patients. Emerging evidence indicates that anemia-driven iron depletion impairs $CD8^+$ T-cell metabolism and function, creating an immunosuppressive microenvironment that compromises T-cell fitness and immunotherapy response, whereas elevated ferritin predicts poor prognosis, pointing to iron metabolism as a promising therapeutic target [45, 46].

This study possesses several strengths that enhance the validity and generalizability of its findings. First, the integrative approach combining high-resolution transcriptomic data with comprehensive clinical phenotyping enables the cross-validation of molecular discoveries within a clinically relevant context. Second, the use of unsupervised clustering and machine learning methods reduces subjective bias and enhances the robustness of the identified signatures. Third, the focus on immunometabolic biomarkers—both at the transcriptomic level and through routine clinical parameters—addresses an important gap in current prognostic models and offers practical tools for risk stratification. Fourth, the inclusion of comprehensive survival analyses with both univariate and multivariate Cox regression, complemented by Kaplan-Meier visualization, provides a rigorous evaluation of prognostic factors.

Nevertheless, several limitations must be acknowledged when interpreting our findings. First, the clinical cohort, while well-characterized, is derived from a single center with a relatively modest sample size (n = 101), which may limit the generalizability of the results and preclude extensive subgroup analyses. Second, the retrospective design may introduce selection bias and reliance on medical records for data ascertainment; therefore, prospective validation in larger, multicenter cohorts is warranted. Third, the survival data, while adequate for the primary analyses, had a median follow-up of 27.9 months, which may be insufficient to capture long-term outcomes in a disease with highly variable survival trajectories. Fourth, the transcriptomic data were derived from a single publicly available dataset (GSE24080); although this dataset is well-annotated and widely used, validation in independent cohorts would strengthen the generalizability of the molecular signatures. Fifth, the 12-gene classifier, while demonstrating excellent diagnostic performance, requires prospective validation and standardization prior to clinical implementation. Sixth, the prognostic findings are based on a cohort from the pre-CAR-T era and may not be extrapolated to patients receiving cellular therapy; future studies should integrate these data with immunometabolic biomarkers for comprehensive risk stratification.

These limitations highlight significant avenues for future research. Prospective cohort studies with extended follow-up are necessary to validate the prognostic value of the identified immunometabolic signatures and to assess their utility in guiding treatment decisions. The integration of cytogenetic and molecular genetic data with immunometabolic biomarkers could enable the development of more comprehensive prognostic models that capture the full complexity of MM biology. Functional studies exploring the mechanistic basis of the observed correlations—for example, how β_2-MG directly or indirectly suppresses erythropoiesis—could identify novel therapeutic targets. The 12-gene classifier should be evaluated in independent cohorts using standardized platforms to assess its reproducibility and clinical utility. Finally, validation of the 12-gene classifier in ISS stage II–III MM patients may address the unmet clinical needs in current risk stratification.

5. CONCLUSIONS

In conclusion, this integrative study demonstrates that MM is characterized by coordinated dysregulation of immunometabolic pathways, with transcriptomic alterations in the p53 and FOXO signaling pathways, profound changes in immune cell composition, and the presence of distinct molecular subtypes. These molecular findings are validated by clinical cohort analysis, which identifies β_2-MG and HGB as independent prognostic factors that reflect tumor burden and its systemic hematopoietic consequences. The strong correlation between these readily accessible biomarkers and bone marrow plasma cell infiltration underscores their utility as practical surrogates for disease burden. Our findings suggest that incorporating immunometabolic biomarkers into existing prognostic frameworks could enhance risk stratification and inform personalized therapeutic strategies in MM. Future prospective studies are warranted to validate these findings and to explore the therapeutic implications of targeting immunometabolic pathways in this heterogeneous disease.

ACKNOWLEDGMENTS

None

AUTHOR CONTRIBUTIONS

Hongqi Yang and Chao Ma designed the study. Song Jin and Lijun Song collected the data and performed the analyses. Song Jin, Qian Xu, Yuping Wei, and Haitao Wang interpreted the data and wrote the manuscript. Tiantian Zhang and Li Wang contributed to the data collection. All authors had final responsibility for the decision to submit the manuscript for publication.

ETHICS STATEMENT

The study was conducted according to the guidelines of the

Declaration of Helsinki, and approved by the Ethics Committee of People's Hospital of Ningxia Hui Autonomous Region (Approval No. 2025-WJW-033; date of approval: February 28, 2025).

INFORMED CONSENT STATEMENT

Informed consent was obtained from all subjects involved in the study.

CONFLICT OF INTEREST STATEMENT

The authors declare no conflicts of interest.

DATA AVAILABILITY STATEMENT

The data that support the findings of this study are available from the corresponding author upon reasonable request.

REFERENCES

1. Kumar SK, Rajkumar V, Kyle RA, et al. Multiple myeloma. *Nat Rev Dis Primers*. 2017;3:17046. DOI: 10.1038/nrdp.2017.46.
2. Zanwar S, Rajkumar SV. Measurable residual disease assessment in multiple myeloma. *Leukemia*. 2026;40(1):25–28. DOI: 10.1038/s41375-025-02830-0.
3. Zanwar S, Kumar S, Rajkumar SV. Diagnosis, risk stratification and management of smouldering multiple myeloma. *Nat Rev Clin Oncol*. 2026;23(4):279–296. DOI: 10.1038/s41571-026-01119-0.
4. Ormond Filho AG, Carneiro BC, Pastore D, et al. Whole-body imaging of multiple myeloma: diagnostic criteria. *Radiographics*. 2019;39(4):1077–1097. DOI: 10.1148/rg.2019180096.
5. Panda T, Aggarwal M, Mallick S, et al. Hypercalcaemia, renal failure, anaemia and osteolytic lesions (CRAB) in chronic lymphocytic leukaemia mimicking multiple myeloma. *BMJ Case Rep*. 2021;14(3):e238864. DOI: 10.1136/bcr-2020-238864.
6. Besliu C, Tanase AD, Rotaru I, et al. The evolving landscape in multiple myeloma: from risk stratification to T cell-directed advanced therapies. *Cancers (Basel)*. 2025;17(3):525. DOI: 10.3390/cancers17030525.
7. Sheykhhasan M, Ahmadieh-Yazdi A, Vicidomini R, et al. CAR T therapies in multiple myeloma: unleashing the future. *Cancer Gene Ther*. 2024;31(5):667–686. DOI: 10.1038/s41417-024-00750-2.
8. Hicks LK, Messersmith HJ, Al Hadidi S, et al. Treatment of multiple myeloma: ASCO-Ontario Health (Cancer Care Ontario) living guideline. *J Clin Oncol*. 2026;44(10):914–941. DOI: 10.1200/JCO-25-02587.
9. Dimopoulos MA, Terpos E, Boccadoro M, et al. EHA-EMN Evidence-Based Guidelines for diagnosis, treatment and follow-up of patients with multiple myeloma. *Nat Rev Clin Oncol*. 2025;22(9):680–700. DOI: 10.1038/s41571-025-01041-x.
10. Greipp PR, San Miguel J, Durie BG, et al. International staging system for multiple myeloma. *J Clin Oncol*. 2005;23(15):3412–3420. DOI: 10.1200/JCO.2005.04.242.
11. Palumbo A, Avet-Loiseau H, Oliva S, et al. Revised International Staging System for multiple myeloma: a report from International Myeloma Working Group. *J Clin Oncol*. 2015;33(26):2863–2869. DOI: 10.1200/JCO.2015.61.2267.
12. Avet-Loiseau H, Durie BG, Cavo M, et al. Combining fluorescent in situ hybridization data with ISS staging improves risk assessment in myeloma: an International Myeloma Working Group collaborative project. *Leukemia*. 2013;27(3):711–717. DOI: 10.1038/leu.2012.282.
13. Cho H, Yoon DH, Lee JB, et al. Comprehensive evaluation of the revised international staging system in multiple myeloma patients treated with novel agents as a primary therapy. *Am J Hematol*. 2017;92(12):1280–1286. DOI: 10.1002/ajh.24891.
14. Neri P, Lee H, Bahlis NJ. Artificial intelligence individualized risk classifier in multiple myeloma. *J Clin Oncol*. 2024;42(11):1207–1210. DOI: 10.1200/JCO.23.02781.
15. D'Agostino M, Cairns DA, Lahuerta JJ, et al. Second revision of the International Staging System (R2-ISS) for overall survival in multiple myeloma: a European Myeloma Network (EMN) report within the HARMONY project. *J Clin Oncol*. 2022;40(29):3406–3418. DOI: 10.1200/JCO.21.02614.
16. Schavgoulidze A, Lauwers-Cances V, Perrot A, et al. Heterogeneity in long-term outcomes for patients with Revised International Staging System stage II, newly diagnosed multiple myeloma. *Haematologica*. 2023;108(5):1374–1384. DOI: 10.3324/haematol.2021.280566.
17. Cao Y, Gong Y, Zhou X, et al. Prognostic evaluation and staging optimization of the Mayo Additive Staging System (MASS) in real world for newly diagnosed multiple myeloma patients. *Hematology*. 2023;28(1):2208914. DOI: 10.1080/16078454.2023.2208914.
18. Sutanto H, Sandra DY, Safira A, et al. Genetic, epigenetic, and molecular determinants of multiple myeloma and precursor plasma cell disorders: a pathophysiological overview. *Med Oncol*. 2025;42(7):234. DOI: 10.1007/s12032-025-02807-0.
19. Iannozzi NT, Giuliani N, Storti P. Deciphering the bone marrow microenvironment's role in multiple myeloma immunotherapy resistance. *Front Immunol*. 2025;16:1613265. DOI: 10.3389/fimmu.2025.1613265.
20. Bai J, Nishimura N, Kawano Y. Advances in immune microenvironment profiling during multiple myeloma progression and therapy. *Int J Hematol*. 2025. DOI: 10.1007/s12185-025-04110-0.
21. Guadagno L, Schütt J, Brinkert K, et al. The role of the bone marrow microenvironment in disease progression and drug resistance in multiple myeloma in the era of novel agents. *Leuk Lymphoma*. 2026;67(1):40–54. DOI: 10.1080/10428194.2025.2575438.
22. Xue HY, Wei F. TGF-beta: an active participant in the immune and metabolic microenvironment of multiple myeloma : TGF-beta in the microenvironment of multiple myeloma. *Ann Hematol*. 2024;103(11):4351–4362. DOI: 10.1007/s00277-024-05843-4.
23. Seymour F, Carmichael J, Taylor C, et al. Immune senescence in multiple myeloma-a role for mitochondrial dysfunction. *Leukemia*. 2022;36(10):2368–2373. DOI: 10.1038/s41375-022-01653-7.
24. Skerget S, Penaherrera D, Chari A, et al. Comprehensive molecular profiling of multiple myeloma identifies refined copy number and expression subtypes. *Nat Genet*. 2024;56(9):1878–1889. DOI: 10.1038/s41588-024-01853-0.
25. Chen X, Luo T, Zhang W, et al. Genomic characteristics and prognostic correlations in Chinese multiple myeloma patients. *BMC Med Genomics*. 2025;18(1):50. DOI: 10.1186/s12920-025-02116-5.
26. Shaughnessy JD Jr, Zhan F, Burington BE, et al. A validated gene expression model of high-risk multiple myeloma is defined by deregulated expression of genes mapping to chromosome 1. *Blood*. 2007;109(6):2276–2284. DOI: 10.1182/blood-2006-07-038430.
27. Kuiper R, Broyl A, de Knegt Y, et al. A gene expression signature for high-risk multiple myeloma. *Leukemia*. 2012;26(11):2406–2413. DOI: 10.1038/leu.2012.127.
28. Jovanović KK, Escure G, Demonchy J, et al. Deregulation and targeting of TP53 pathway in multiple myeloma. *Front Oncol*. 2019;8:665. DOI: 10.3389/fonc.2018.00665.

29. Bloedjes TA, de Wilde G, Maas C, et al. AKT signaling restrains tumor suppressive functions of FOXO transcription factors and GSK3 kinase in multiple myeloma. *Blood Adv*. 2020;4(17):4151–4164. DOI: 10.1182/bloodadvances.2019001393.
30. Bloedjes TA, de Wilde G, Khan GH, et al. AKT supports the metabolic fitness of multiple myeloma cells by restricting FOXO activity. *Blood Adv*. 2023;7(9):1697–1712. DOI: 10.1182/bloodadvances.2022007383.
31. Uckun FM. Overcoming the immunosuppressive tumor microenvironment in multiple myeloma. *Cancers (Basel)*. 2021;13(9):2018. DOI: 10.3390/cancers13092018.
32. Moscvin M, Evans B, Bianchi G. Dissecting molecular mechanisms of immune microenvironment dysfunction in multiple myeloma and precursor conditions. *J Cancer etastasis Treat*. 2023;9:17. DOI: 10.20517/2394-4722.2022.110.
33. Hadjiaggelidou C, Katodritou E. Regulatory T-cells and multiple myeloma: implications in tumor immune biology and treatment. *J Clin Med*. 2021;10(19):4588. DOI: 10.3390/jcm10194588.
34. Dahlhoff J, Manz H, Steinfatt T, et al. Transient regulatory T-cell targeting triggers immune control of multiple myeloma and prevents disease progression. *Leukemia*. 2022;36(3):790–800. DOI: 10.1038/s41375-021-01422-y.
35. Cencini E, Sicuranza A, Ciofini S, et al. Tumor-associated macrophages in multiple myeloma: key role in disease biology and potential therapeutic implications. *Curr Oncol*. 2023;30(7):6111–6133. DOI: 10.3390/curroncol30070455.
36. Zhang YJ, Cao QH, Yang YH. Effect of JMJD3-IRF4 signaling pathway-mediated macrophage polarization on the malignant biological behavior of multiple myeloma cells. *J Exp Hematol*. 2024;32(5):1455–1462. Chinese. DOI: 10.19746/j.cnki.issn.1009-2137.2024.05.024.
37. Mougiakakos D, Bach C, Böttcher M, et al. The IKZF1-IRF4/IRF5 axis controls polarization of myeloma-associated macrophages. *Cancer Immunol Res*. 2021;9(3):265–278. DOI: 10.1158/2326-6066.CIR-20-0555.
38. Sabol HM, Ashby C, Adhikari M, et al. A NOTCH3-CXCL12-driven myeloma-tumor niche signaling axis promotes chemoresistance in multiple myeloma. *Haematologica*. 2024;109(8):2606–2618. DOI: 10.3324/haematol.2023.284443.
39. Shu P, Guo F, Qin D, et al. CXCR4-modification enhances CAR-T efficacy by improving tumor tracking and bone marrow homing in B-cell malignancies. *Signal Transduct Target Ther*. 2026;11(1):38. DOI: 10.1038/s41392-025-02522-2.
40. Chiou SJ, Chen CH. Decipher beta2-microglobulin: gain- or loss-of-function (a mini-review). *Med Sci Monit Basic Res*. 2013;19:271–273. DOI: 10.12659/MSMBR.889457.
41. Grzaśko N. Involvement of apoptosis and proinflammatory cytokines in the pathogenesis of anemia in multiple myeloma. *Postepy Hig Med Dosw (Online)*. 2004;58:364–371. Polish. https://pubmed.ncbi.nlm.nih.gov/15536394/.
42. Rokicka-Piotrowicz M, Paszkowska M, Król M, et al. Analysis of causes for anemia in patients with multiple myeloma. *Pol Arch Med Wewn*. 2000;104(6):843–851. Polish. https://pubmed.ncbi.nlm.nih.gov/11424663/.
43. Fotiou D, Katodritou E. From biology to clinical practice: the bone marrow microenvironment in multiple myeloma. *J Clin Med*. 2025;14(2):327. DOI: 10.3390/jcm14020327.
44. Brigle K, Pierre A, Finley-Oliver E, et al. Myelosuppression, bone disease, and acute renal failure: evidence-based recommendations for oncologic emergencies. *Clin J Oncol Nurs*. 2017;21(5 Suppl):60–76. DOI: 10.1188/17.CJON.S5.60-76.
45. Xu P, Huang C, Liu Y, et al. Peripheral blood inflammatory ratios predict efficacy and toxicity of CAR-T cell immunotherapy in relapsed/refractory multiple myeloma. *Front Immunol*. 2026;17:1752235. DOI: 10.3389/fimmu.2026.1752235.
46. Teh MR, Gudgeon N, Frost JN, et al. Iron deficiency causes aspartate-sensitive dysfunction in CD8(+) T cells. *Nat Commun*. 2025;16(1):5355. DOI: 10.1038/s41467-025-60204-7.

How to cite this article: Jin S, Song LJ, Xu Q, Zhang TT, Wang L, Wei YP, et al. Integrative transcriptomic and clinical cohort analysis identifies immunometabolic prognostic signatures in multiple myeloma. *J Blood Biother*. 2026;1(1):1–15. DOI: 10.46701/jbbt260502.